

Shear Assessment and Strengthening of Contiguous-Beam Concrete Bridges Using FRP Bars

by P. Valerio, T.J. Ibell and A.P. Darby

Synopsis: Many concrete bridges related to railways in the U.K. consist of prestressed rectangular concrete beams, post-tensioned together transversely to aid lateral distribution of load; this bridge type has been repeatedly flagged as having insufficient shear capacity. Sixteen tests on small-scale beams, which are scaled-down replica models of the actual bridge beams, are presented. The specimens are tested under a four-point loading system and are both prestressed (PRC) with and without stirrups and non-prestressed (RC) with and without stirrups, to provide full understanding of their shear behaviour. Four further tests are then presented on RC beams strengthened in shear with FRP bars inserted from the soffit into pre-drilled holes and fixed in place using epoxy resin; this method allows strengthening in cases where the webs are inaccessible. Comparisons are made with current code predictions for the strength of all specimens. The results show that unstrengthened RC beams behave mostly as expected and as predicted by codes, while for PRC beams a great variation in shear-carrying capacity following shear cracking is observed for different span-to-depth loading ratios. The proposed FRP strengthening scheme is effective and provides significant improvement to the shear-carrying load capacity.

Keywords: bridges; fiber-reinforced polymers; prestressed concrete; reinforced concrete; shear; strengthening

826 Valerio et al.

Pierfrancesco Valerio is a Research Officer in the Department of Architecture and Civil Engineering at the University of Bath, UK, where he started a PhD in Structural Engineering in October 2003. He received his MEng in Italy in 2001 and worked as a consultant in an Italian bridge design company from 2001 to 2003. He is a Professional Engineer in Italy since 2002. His interests and fields of expertise include the design of steel and concrete structures and bridge engineering.

Tim Ibell is an ACI Member. He obtained his PhD from the University of Cambridge, UK, in 1992. Tim is now Chair of the Department of Architecture and Civil Engineering at the University of Bath, UK. His research interests include the internal prestressing and strengthening of concrete structures using fiber-reinforced polymer materials.

Antony Darby is a Lecturer in Structural Engineering at the Department of Architecture and Civil Engineering, University of Bath, UK. He obtained his PhD from Cambridge University and spent two years at Oxford University gaining post-doctorial research experience. He has also worked in Industry for a number of years as a Design Engineer. His research interests are in FRP strengthening and structural dynamics.

INTRODUCTION

Due to increased traffic, higher allowable truck weights and deterioration of materials, most bridges in the U.K. have been assessed recently for both bending and shear capacity. A steady-state assessment program of these bridges is now moving into place. During this process, various bridge owners have identified two areas of concern which need to be addressed: the first is the realistic shear strength assessment of prestressed concrete bridge beams when made contiguous within a deck, and the second is the necessity for quick, cheap and practical shear strengthening measures for such bridges when the webs of the beams are inaccessible.

As plasticity-based yield line methods for flexural strength assessment of concrete bridges become ever more popular, so the demand on shear strength in these bridges increases, leading to many shear assessment failures. The priority is therefore to ensure that a realistic shear assessment tool is in place, which is able to predict the real strength of such bridges adequately. Thereafter, if it turns out that the bridge has inadequate shear strength, a viable shear strengthening scheme is sought, which ensures minimal disruption to the bridge users. By combining these two aspects in one project, a powerful management tool for owners of concrete bridges with shear concerns will be produced.

The shear assessment tool will be achieved through large- and small-scale tests combined analytically with a plasticity-based shear assessment method for beams, slabs and beam-and-slab bridges developed previously⁽¹⁾, and through laboratory testing of the same specimens, but in the strengthened situation.

There are several approaches to retrofitting existing concrete bridges in shear⁽²⁾, often involving the use of FRP laminates fixed to the webs of the bridge beams or FRP bars

mounted near the surface of the webs⁽³⁾. However, in the particular case where the webs of the beams are inaccessible, an altogether new approach must be adopted. Vertical holes are drilled into the bridge beams from the soffit level. FRP bars are then inserted and embedded in place using high-viscosity epoxy resin injected into the drilled holes. In this way, shear enhancement is shown to be possible.

In this paper, the tests on unstrengthened small-scale beams (which are replica scaled-down models of actual bridge beams) are presented alongside four further tests on RC beams strengthened in shear with FRP bars using the technique described above. Comparisons are made against current code predictions for the strength of all specimens in both the unstrengthened and strengthened situations.

The next step in this research project will be the completion of tests on complete small-scale bridge specimens as well as large-scale beams, along with the validation of the proposed FRP-strengthening technique for PRC beams, small-scale bridge specimens and large-scale beams.

EXPERIMENTAL PROGRAM

Design of the test specimens

The existing bridge taken as a reference for the construction of the test specimens for assessing the unstrengthened situation is a simply-supported railway underbridge consisting of ten pre-tensioned rectangular concrete beams transversely post-tensioned together to form a deck (see Figure 1). Each beam, whose minimum concrete compressive cube strength at 28 days is 60MPa, is 900mm wide and 762mm deep and is pre-tensioned longitudinally with a total of 38 tendons at mid-span (21 of which are debonded towards the support): each tendon is stressed to an initial force of 159kN (see Figure 2). The percentage of transverse reinforcement equals 0.35% at support, 0.175% in the shear zone and 0.098% in the middle zone of the beam.

Sixteen small-scale specimens were designed in such a way as to match, as much as possible, the average values in the shear zone of the real beams in terms of geometric and sectional characteristics (effective depth to total depth ratio, percentage of longitudinal and transverse reinforcement) and in terms of tension state due to the prestressing forces and permanent loads. The beams were 110mm wide, 190mm deep and 3000mm long, with four 7mm wires (of which only the upper two were pre-tensioned to 45kN each, in the case of the PRC beams) as longitudinal reinforcement and 3mm mild steel bars as vertical stirrups, whose spacing was 175mm in the central zone, 100mm in the shear zone and 50mm at the support (see Figures 2 and 3).

Four RC specimens were then designed in order to verify the feasibility of the proposed shear strengthening scheme. The FRP reinforcement used was 10mm diameter aramid ARAPREE⁽⁴⁾ bars with a tensile strength of 1.5GPa, Young's modulus of 60GPa, ultimate strain of 2.4% and density of 12.5kN/m³. These beams were 110mm wide,

220mm deep and 3000mm long, with no stirrups and two 12mm high yield steel bars as longitudinal reinforcement (see Figure 4).

Test program

All beams were tested under a four-point loading system with a hinge and roller respectively at each end, to provide constant shear within the shear spans. For the sixteen unstrengthened small-scale specimens the load position was varied along the length of the beam, at 3, 4, 5 and 6 times the effective depth d of the beam, to ensure that a range of shear span lengths was examined. Furthermore, to understand the numerous parameters involved in the shear-carrying capacity of concrete beams (especially if prestressed), they were tested in all their four different configurations, i.e. prestressed with stirrups (PRCst), prestressed without stirrups (PRC), non-prestressed with stirrups (RCst) and non-prestressed without stirrups (RC). Figure 5 shows the test layout of the sixteen unstrengthened small-scale beams (USB).

All four beams to be FRP-strengthened were non-prestressed without stirrups (RC) and were tested at 3 times their effective depth. The first specimen contained no FRP bars, while the second, third and fourth specimens contained, respectively, three, two and one ARAPREE bars in each shear span, as shown in Figure 6 (where SB stands for strengthened beams).

Casting and testing procedure

The beams were cast in a steel formwork, which forms the prestressing rig for the PRC beams (see Figure 7). The prestressing force load was applied by a 200kN hydraulic jack bearing against the end plate and each jack was tensioned to 45kN. The characteristic compressive cube strength required for the concrete was 60MPa. For the beams due to be strengthened, two weeks after casting the required holes were drilled in the shear spans and the FRP bars were inserted and epoxy-resined into place.

The loading arrangement for the tests is shown in Figure 8. The loads were applied on the beams via two steel bearings loaded by 100kN hydraulic jacks, whose reactions were provided by a rigid steel beam, itself supported over two rigid transversal steel frames. Prior to testing, six displacement transducers were set on each specimen to obtain the load-displacement plots. All beams were loaded monotonically until failure, with crack patterns marked throughout the testing procedure. The readings from the transducers were taken every second with a measurement group System 500 data logger.

TEST RESULTS AND DISCUSSION

Samples of the 7mm prestressing wires, the 3mm mild steel bars used for the stirrups and of the 12mm high yield steel bars for the FRP-strengthened specimens were tested in tension and the corresponding stress-strain plots were obtained. Average values of 1610MPa, 700MPa and 635MPa were found for the tensile strength of the wires and the yield stress of the 3mm and 12mm bars respectively.

Tests on the unstrengthened small-scale beams

Table 1 summarizes the results of the sixteen tests on the unstrengthened small-scale beams; f_{cu} is the average of the characteristic value of the compressive cube strength of the four cubes tested for each beam. Figures 9 to 28 show pictures at failure and the load-displacement plots for each beam.

The four RC beams, which all failed in shear, behaved similarly in terms of peak load and maximum deflection, and the failure load in all cases was just slightly higher (4 to 10%) than the first shear cracking load, demonstrating that for a non-prestressed beams without stirrups the first shear cracking initiates beam collapse. A reduction in the ultimate failure load of about 15% was noted for the beams loaded at $5d$ and $6d$ with respect to the ones loaded at $3d$ and $4d$, showing a tendency for the ultimate shear failure load to decrease with the shear span length. The four RC beams with stirrups, which again all failed in shear, behaved similarly in terms of peak load and maximum deflection, and their failure load was 6.7 to 8.7kN higher than the failure load of the equivalent beams without stirrups, showing an average increase of 7.6kN in the ultimate carrying capacity due to the presence of the stirrups.

The four PRC beams without stirrups all failed in shear, but this time with notable differences in terms of peak load, maximum displacement and stiffness. A great enhancement in stiffness, shear carrying capacity and maximum displacement was observed as the shear span length reduced; the peak load ranged from 28.5kN (at $6d$) to 54.1kN (at $3d$), (a remarkable 90% increase), while at $4d$ and $5d$ the peak load was 37.5 and 31.3kN respectively, values in between the two extremes. When compared with the equivalent non-prestressed beams, the enhancement in shear capacity due to the prestressing effect reduced greatly with the shear span length, ranging from 230% at $3d$ to 31% at $6d$. In these four prestressed beams, the shear failure load was substantially higher than the first shear cracking load, proving the existence of an arching action of the prestressing force which helps the shear carrying mechanism. Furthermore, the first shear cracks for the beam loaded at $6d$ appeared at a load of 21kN, just 1kN more than the non-prestressed case, showing that for such high shear slenderness the enhanced shear capacity of prestressed beams can only be related to the previously mentioned arch action.

The four PRC beams with stirrups all failed in flexure, apart from the one loaded at $3d$, which failed in shear at 54.5kN, a value practically coincident with the equivalent PRC beam without stirrups. A strong reduction in stiffness with increasing shear span length was noted for these four beams. The stirrups in the beams loaded at 4, 5 and 6 times d were able to change the failure mode from brittle shear to ductile flexure and, therefore, were very effective. The lack of enhancement of capacity in the beam loaded at $3d$ was probably due to the fact that, for such high loads, amongst the three shear carrying mechanisms that interact in PRC beams with stirrups (namely the concrete, the stirrups and the arch action contributions), the arch action is dominant. Once this action expires the load level is so high that the stirrups cannot be effective anymore. In the beam loaded at $6d$ the flexural failure was not as ductile as the other two: signs of shear failure were observed in the test specimen, again confirming the tendency for the ultimate shear failure load to decrease with the shear span length.

Tests on the FRP-strengthened beams

Table 2 summarizes the results of the four tests on the FRP-strengthened beams, while Figures 29 to 33 show their the load-displacement plots and pictures at failure.

The plain control specimens (SB 1) failed in brittle shear at 23kN. The beam strengthened with 3 bars (SB 2) failed in flexure at 41.5kN, while the ones with two and one FRP bar (SB 3 and SB 4) failed in shear at 32kN and 30kN respectively. The strengthening was clearly effective. With respect to the plain specimen, the three FRP bars contained in beam SB 2 altered the failure mechanism leading from a brittle shear to a ductile flexural failure, increasing considerably the ultimate load capacity and ductility of the beam. Again, the increase in ultimate capacity was remarkable even in specimens SB 3 and SB 4, which failed in shear but with a 40% and 30% increase respectively when compared to beam SB 1.

Looking at the shape of the shear cracks that led to failure in SB 1 and SB 3, it is clear that the slope of the shear discontinuity in beam SB 3 was steeper than that in SB 1: the presence of the bars forced the shear discontinuity to be steeper and form within the constricted space between the vertical bars. This permitted greater internal energy dissipation in the failure mechanism, leading to a higher ultimate load capacity.

ANALYSIS OF TEST RESULTS**Flexural analysis**

Following the symbols of EC2⁽⁵⁾, in the uncracked phase the theoretical first cracking load for all beams is given by:

$$P_{cr} = \frac{M_{cr}}{a} = \frac{I}{a y_{bot}} (f_{ctm} + \sigma_{cp,bot}) \quad (1)$$

where $f_{ctm} = 0.3f_{ck}^{2/3}$ is the mean value of the axial tensile strength of concrete, f_{ck} is the characteristic compressive cylinder strength of concrete, $\sigma_{cp,bot}$ is the stress due to prestressing force at the bottom fibre of the section after all the prestressing losses, I is the transformed second moment of area of the cross-section, y_{bot} is the distance from the centroid to the bottom fibre and a is the shear span length.

At the ultimate limit state, assuming all partial safety factors equal to unity, the theoretical ultimate load is given by:

$$P_{ult} = \frac{M_{ult}}{a} = \frac{(C_u \cdot 0.6x) + \sum T_{s,i} (d_i - x)}{a} \quad (2)$$

where C_u is the ultimate compressive force in concrete, x is the depth to the neutral axis, d_i is the effective depth of each steel layer and T_i is the ultimate force in each steel layer.

Table 3 shows the correlation between the flexural analysis and test results; it is evident that both the theoretical first flexural cracking load and the ultimate load (when applicable, i.e. for the specimens which failed in flexure) produce very accurate predictions, with a maximum discrepancy of 3% for the ultimate load and 10% for the cracking load.

Shear predictions from codes of practice

Comparisons between the ultimate load observed and code predictions are now made for all beams. Codes-of-practice EC2⁽⁵⁾, BS 8110-1⁽⁶⁾, BD 44/95⁽⁷⁾ and DIN 1045-1⁽⁸⁾ are used for comparison purposes.

In determining the ultimate shear capacity of the beams strengthened with FRP bars, the term V_f (the shear strength contribution from the FRP) is added to the concrete contribution V_c . It is assumed that the vertically-embedded FRP bars will strain to 0.004 at the ultimate shear capacity of the beams⁽³⁾. With a Young's modulus of the FRP bars of 60GPa, the limit stress in the FRP bars at shear collapse is 240MPa. Thus, the term for V_f , based on a 45° truss analogy, is:

$$V_f = \frac{240 A_f z}{s_v} \quad (3)$$

where A_f is the cross-sectional area of each bar, z is the effective lever arm of the truss and s_v is the spacing between vertical bars.

Although the codes-of-practice adopted here limit the spacing between stirrups to various fractions of the effective depth, d , the calculations conducted here ignore this limitation. Naturally, the design of an adequate shear-strengthening scheme would require closely-spaced vertical bars in reality. The value of z is taken to be the fully-anchored length of each embedded bar, which is the overall length of each bar minus the anchorage length at each end. It is assumed that the average bond strength between epoxy-resined bar and concrete (where $\tau_{av}=0.5\tau_{max}$ with a triangular stress distribution) is of the order of 12MPa⁽⁹⁾. This translates to an anchorage length, l_b , of 50mm for the 10mm diameter bars, so $z=h-2l_b=120$ mm.

Table 4 shows details of comparison between the various code predictions and the actual results. For the unstrengthened specimens, all codes give good correlation for the RC beams; for RC beams with stirrups the predictions of BS 8810-1 and BD 44/95 are good, while EC2 and DIN 1045-1, which consider a variable angle truss model, are close to actual only if considering the minimum allowed inclination θ of the compression struts (for DIN 1045-1 the suggested value of $\theta=40^\circ$ is considered in the Table, resulting in very conservative predictions). For PRC beams, EC2 and DIN 1045-1 give good predictions for long shear spans, but are too conservative for short shear spans. BS 8110-1 and BD 44/95 are very conservative for PRC beams. For PRC beams with stirrups all predictions are extremely conservative and poor, because no code is able to catch the flexural failure. Only DIN 1045-1 predictions are reasonable for long shear spans.

All codes-of-practice predict the shear capacity of the FRP-strengthened RC beams reasonably accurately, especially DIN 1045-1, whose predictions are always within a 5% error margin from the actual failure load. However, for specimens SB 3 and SB 3, in particular, there is an overestimation of the effectiveness of the vertical bars. This is almost certainly due to their wide spacing, which is close to one effective depth for specimen SB 3 and substantially more than one effective depth for specimen SB 4. Therefore, clearly it is essential that in order for this strengthening scheme to be efficiently used in reality, the vertically-embedded bars should be spaced sufficiently closely in order for shear predic-

tions to be valid. It seems sensible that this minimum spacing should be in the region of 0.5 to 0.75 times the effective depth (as in SB 2), just as recommended by present codes of practice. However, in specimens SB 3 and SB 4, although the bars were spaced too widely to be fully effective, they enhanced shear capacity by altering the shear discontinuity geometry.

It is then observed that, if considering the average value between all 20 tests, EC2 is the code with the better coefficient of variation, while the poor performance of DIN 1045-1 is caused mostly by the excessively conservative predictions for the RC beams with stirrups.

CONCLUSIONS

With regard to the unstrengthened small-scale beams, it has been shown that the RC beams behaved mostly as expected and as predicted by codes of practice on condition that a minimum value for the inclination of the compression struts is chosen for the beams containing stirrups. For PRC beams, a great variation in shear-carrying capacity after shear cracking is observed when loading with different span-to-depth ratios. In particular the shear capacity decreased greatly with increasing shear span lengths, pointing to the fact that in PRC beams, along with a great shear enhancement near the support, the critical zone for shear failure is located at 5 to 6 times the effective depth. This fact should be considered when providing shear strengthening for PRC beams. For PRC beams, the codes of practice proved to be excessively conservative, especially for the PRC beams containing stirrups.

The proposed shear-strengthening approach has been shown to be feasible and successful for RC beams. The spacing between embedded bars should be close enough so that the shear discontinuity cannot form between bars. It is suggested that existing requirements for maximum spacing of vertical reinforcement, which vary between 0.5 and 0.75 times the effective depth, should be adequate for such strengthening. It can therefore be concluded that it is possible to design a shear-strengthening scheme using embedded FRP bars by assuming the reinforcement contribution according to Eq. (3). Validation of the technique for the case of PRC beams and large-scale beams will be the next task of this research project.

ACKNOWLEDGEMENTS

The authors gratefully acknowledge the help of the laboratory staff and the financial support of the Engineering and Physical Sciences Research Council (EPSRC) and Network Rail.

REFERENCES

1. Ibell, T. J., Morley, C. T. and Middleton, C. R., "A plasticity approach to the assessment of shear in concrete beam-and-slab bridges". *The Structural Engineer*, Vol. 75, No. 19, pp. 331-338, 1997.
2. Concrete Society TR 55, "Design guidance for strengthening concrete structures using fibre composite materials". Second Edition. The Concrete Society, Camberley, UK, 2004.
3. De Lorenzis, L. and Nanni, A., "Shear strengthening of reinforced concrete beams with near-surface mounted fiber-reinforced polymers rods". *ACI Structural Journal*, Vol. 98, No. 1, pp. 60-68, 2001.
4. Sireg SpA, "ARAPREE-CARBOPREE bars". Sireg Geotechnical Division Catalogue, Arcore, Italy, 2001.
5. Eurocode 2: EN 1992-1-1 Final draft, "Design of concrete structures. Part 1-1: General rules and rules for buildings". European Committee for Standardization, 2003.
6. BS 8110-1, "Structural use of concrete. Part 1: Code of practice for design and construction". British Standard Institution, London, 1997.
7. BD 44/95, "The assessment of concrete highway bridges and structures". Department of Transport, London, 1995.
8. DIN 1045-1, "Reinforced an prestressed concrete structures – Part 1: Design". Deutsches Institut für Normung (DIN), Berlin, 2001.
9. De Lorenzis, L. and Nanni, A., "Characterization of FRP rods as near surface mounted reinforcement". *ASCE Journal of Composites for Construction*, Vol. 5, No. 2, pp. 114-121, 2001.

Table 1 – Tests on the unstrengthened small-scale beams

Specimen	Test Layout	f_{cu} (MPa)	P at flex. cracking (kN)	P at shear cracking (kN)	Peak failure load P (kN)	Max span deflection (mm)
USB 1.1	RC@3d	62	6	22.5	23.5 (shear)	25.9
USB 1.2	RCst@3d	54	6	22.5	31.5 (shear)	32.3
USB 1.3	PRC@3d	61	18	34.5	54.1 (shear)	66.5
USB 1.4	PRCst@3d	59	18	34.5	54.5 (shear)	64.3
USB 2.1	RC@4d	59	5.5	23	25.1 (shear)	30.9
USB 2.2	RCst@4d	59	5.5	23	33.8 (shear)	44.4
USB 2.3	PRC@4d	59	15	30	37.5 (shear)	45.6
USB 2.4	PRCst@4d	60	15	30	46.4 (flexure)	91.7
USB 3.1	RC@5d	64	4	20	21.3 (shear)	27.8
USB 3.2	RCst@5d	64	4	20	28.3 (shear)	38.6
USB 3.3	PRC@5d	60	12	26	31.3 (shear)	45.2
USB 3.4	PRCst@5d	64	12	26	37.9 (flexure)	86.1
USB 4.1	RC@6d	60	3	20	21.7 (shear)	34.7
USB 4.2	RCst@6d	54	3	20	28.4 (shear)	44.3
USB 4.3	PRC@6d	63	10	21	28.5 (shear)	42.0
USB 4.4	PRCst@6d	57	10	21	31.2 (flexure)	70.3

Table 2 – Tests on the FRP-strengthened beams

Specimen	Shear zone layout	f_{cu} (MPa)	P at flex. cracking (kN)	P at shear cracking (kN)	Peak failure load P (kN)	Max span deflection (mm)
SB 1	Plain	52	7.5	22.5	22.5 (shear)	12
SB 2	3+3 bars	52	7.5	23	41.5 (flexure)	>40
SB 3	2+2 bars	50	7.5	23	32 (shear)	13
SB 4	1+1 bar	51	7.5	22	30 (shear)	12

Table 3 – Correlation between flexural analysis and test results for all beams

Specimen	Actual P_{cr} (kN)	Predicted P_{cr} (kN)	Actual P_{ult} (kN)	Predicted flex- ural P_{ult} (kN)
USB 1.1	6.0	5.6	23.5 (shear)	63.0
USB 1.2	6.0	5.6	31.5 (shear)	63.0
USB 1.3	18.0	18.0	54.1 (shear)	64.1
USB 1.4	18.0	18.0	54.5 (shear)	64.1
USB 2.1	5.5	4.1	25.1 (shear)	47.1
USB 2.2	5.5	4.1	33.8 (shear)	47.1
USB 2.3	15.0	13.5	37.5 (shear)	48.0
USB 2.4	15.0	13.5	46.4 (flexure)	48.0
USB 3.1	4.0	3.2	21.3 (shear)	37.7
USB 3.2	4.0	3.2	28.3 (shear)	37.7
USB 3.3	12.0	10.8	31.3 (shear)	38.3
USB 3.4	12.0	10.8	37.9 (flexure)	38.3
USB 4.1	3.0	2.6	21.7 (shear)	31.3
USB 4.2	3.0	2.6	28.4 (shear)	31.3
USB 4.3	10.0	9.0	28.5 (shear)	31.9
USB 4.4	10.0	9.0	31.2 (flexure)	31.9
SB 1	7.5	7.6	22.5 (shear)	40.5
SB 2	7.5	7.6	41.5 (flexure)	40.5
SB 3	7.5	7.6	32 (shear)	40.5
SB 4	7.5	7.6	30 (shear)	40.5

Table 4 – Correlation between codes predictions and test results for all beams

Specimen	Actual P_{ult} (kN)	EC 2 P_{ult} (kN)	BS 8110 P_{ult} (kN)	BD 44 P_{ult} (kN)	DIN 1045 P_{ult} (kN)
USB 1.1	23.5 (shear)	21.0	18.6	20.5	17.4
USB 1.2	31.5 (shear)	28.4	27.8	30.6	15.8
USB 1.3	54.1 (shear)	29.5	22.8	26.3	24.2
USB 1.4	54.5 (shear)	28.4	32.6	37.1	39.7
USB 2.1	25.1 (shear)	21.0	18.6	20.5	17.4
USB 2.2	33.8 (shear)	28.4	27.8	30.6	15.8
USB 2.3	37.5 (shear)	29.5	19.8	20.3	24.2
USB 2.4	46.4 (flexure)	28.4	26.4	31.1	39.7
USB 3.1	21.3 (shear)	21.0	18.6	20.5	17.4
USB 3.2	28.3 (shear)	28.4	27.8	30.6	15.8
USB 3.3	31.3 (shear)	29.5	18.1	17.0	24.2
USB 3.4	37.9 (flexure)	28.4	27.9	27.8	39.7
USB 4.1	21.7 (shear)	21.0	18.6	20.5	17.4
USB 4.2	28.4 (shear)	28.4	27.8	30.6	15.8
USB 4.3	28.5 (shear)	29.5	16.9	14.9	24.2
USB 4.4	31.2 (flexure)	28.4	26.7	25.6	39.7
SB 1	23 (shear)	26	24	24.5	22
SB 2	41.5 (flexure)	40.5 (flex)	40.5 (flex)	40.5 (flex)	40.5 (flex)
SB 3	32 (shear)	37	35	36	33
SB 4	30 (shear)	33.5	31.5	32	29.5
Mean ratio of predicted to actual capacity	--	0.895	0.798	0.843	0.785
Average coefficient of variation	--	19.7%	24.1%	24.2%	27.3%

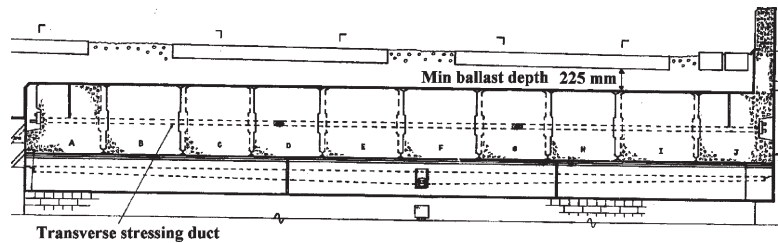


Figure 1 – Cross section of the existing bridge

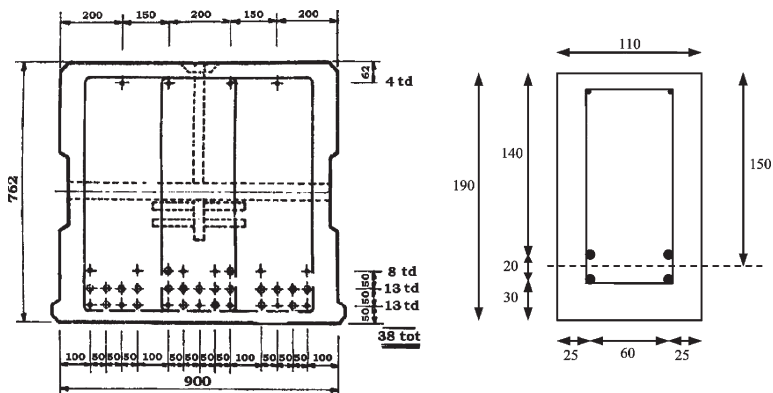


Figure 2 – Cross-section of the existing bridge beams and of the small-scale beams (mm)

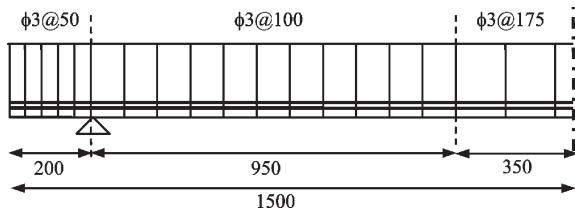


Figure 3 – Half length elevation of the small-scale beams (mm)

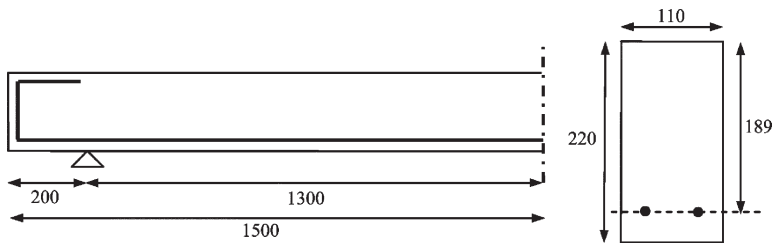


Figure 4 – Half length elevation and cross section of the FRP-strengthened beams (mm)

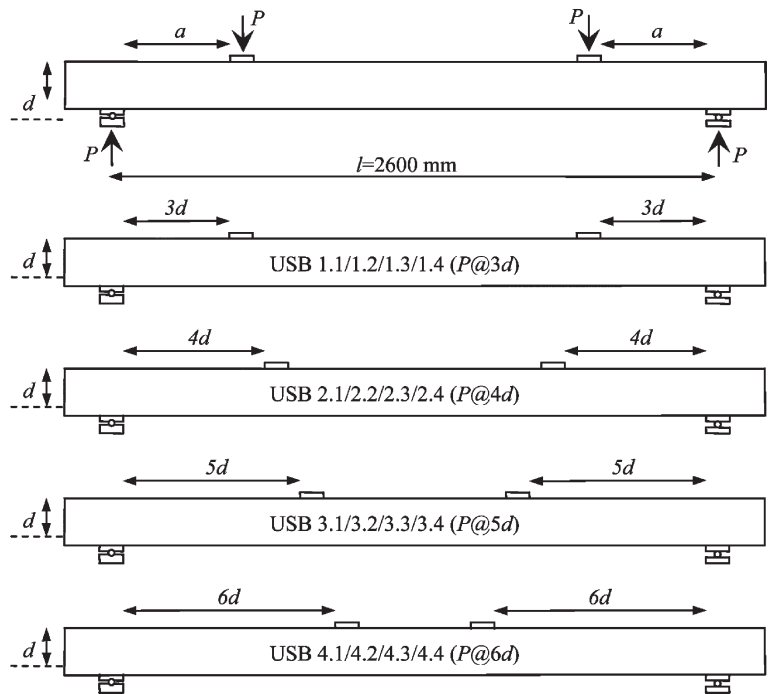


Figure 5 (a) – Test layout for the small-scale beams

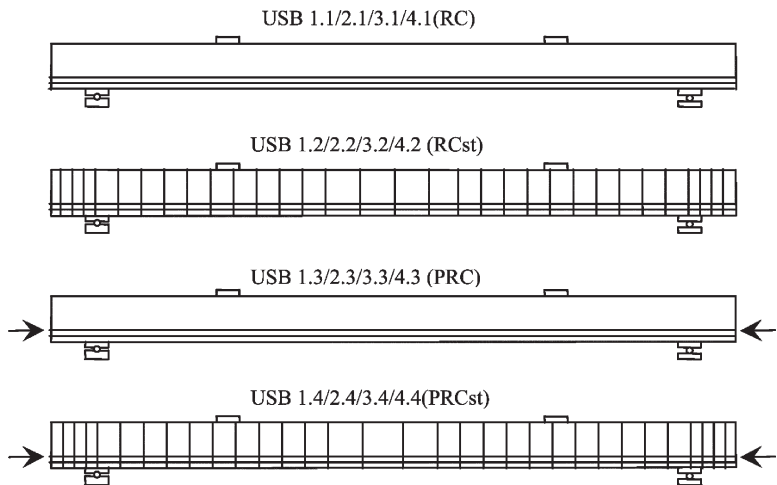


Figure 5 (b) – Test layout for the small-scale beams

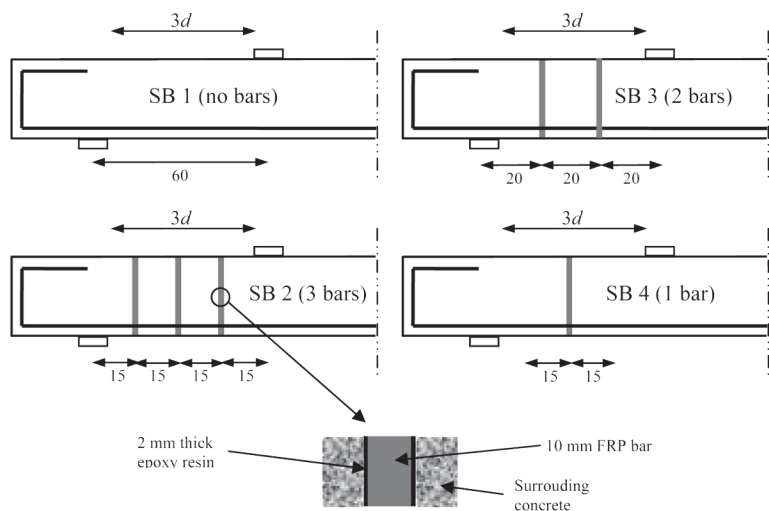


Figure 6 – Test layout for the FRP-strengthened beams

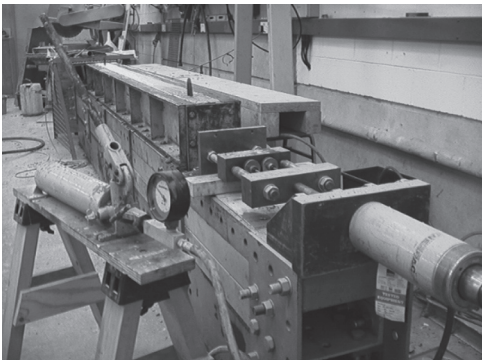


Figure 7 – Casting/prestressing rig

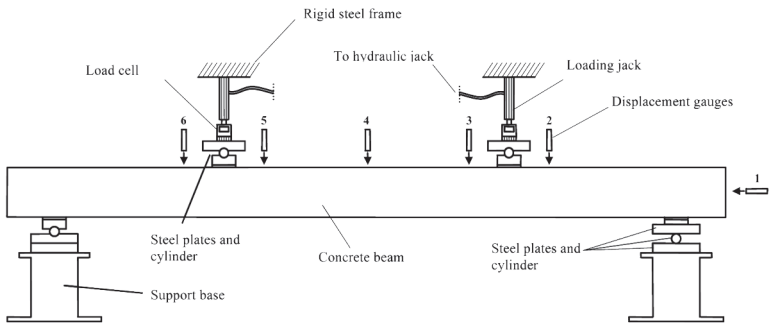


Figure 8 – Test set-up

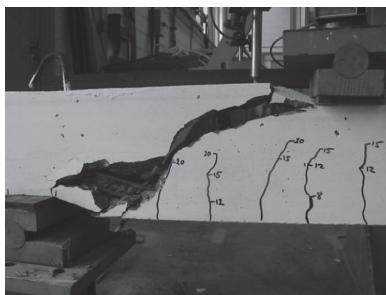


Figure 9 – USB 1.1 at failure

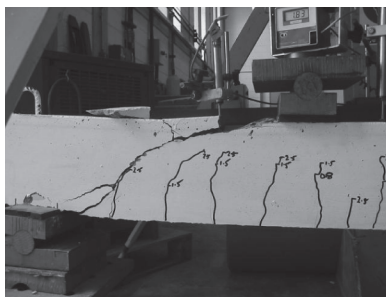


Figure 10 – USB 1.2 at failure



Figure 11 – USB 1.3 at failure

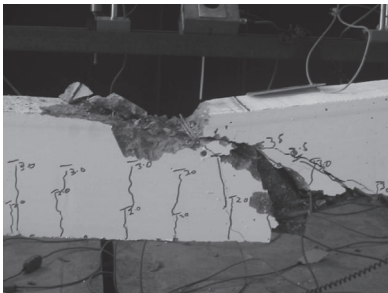


Figure 12 – USB 1.4 at failure

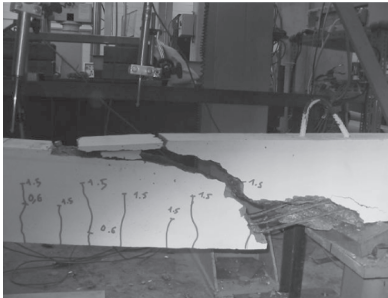


Figure 13 – USB 2.1 at failure

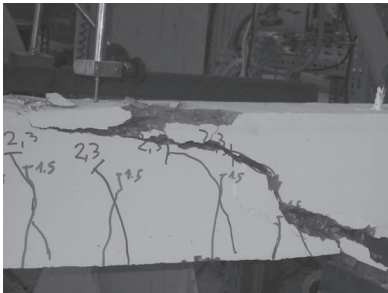


Figure 14 – USB 2.2 at failure

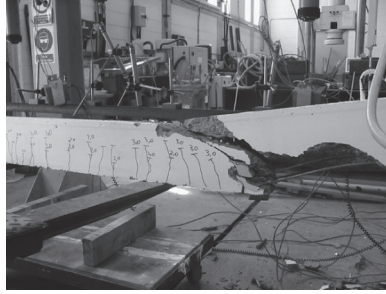


Figure 15 – USB 2.3 at failure

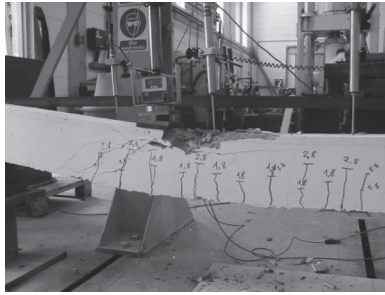


Figure 16 – USB 2.4 at failure



Figure 17 – USB 3.1 at failure



Figure 18 – USB 3.2 at failure

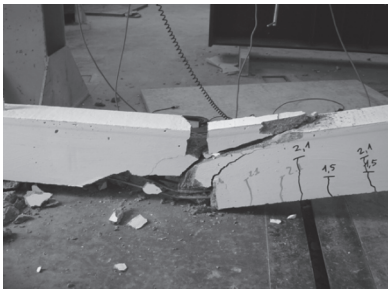


Figure 19 – USB 3.3 at failure



Figure 20 – USB 3.4 at failure



Figure 24 – USB 4.4 at failure

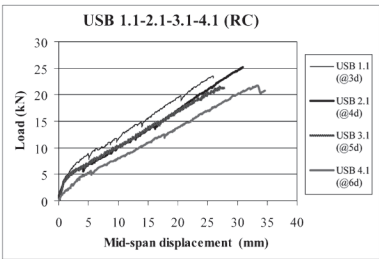


Figure 25 – Load displacement plot for the unstrengthened RC beams

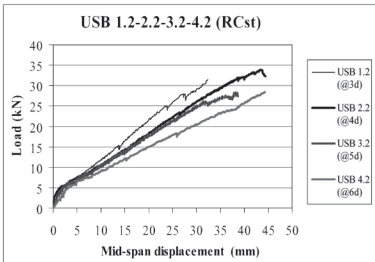


Figure 26 – Load displacement plot for the unstrengthened RC beams with stirrups

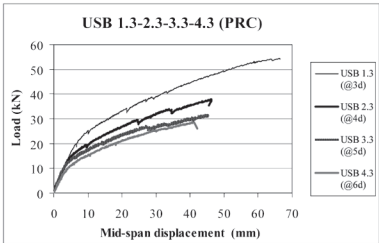


Figure 27 – Load displacement plot for the unstrengthened PRC beams

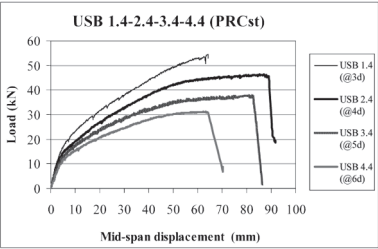


Figure 28 – Load displacement plot for the unstrengthened PRC beams with stirrups

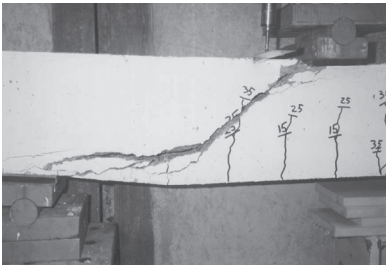


Figure 29 – SB 1 at failure

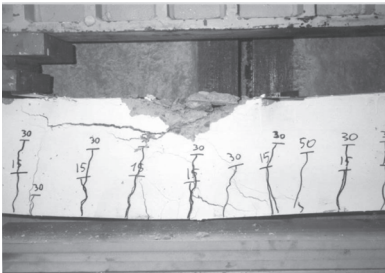


Figure 30 – SB 2 at failure

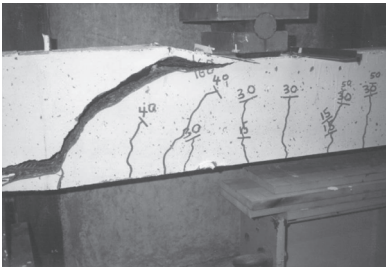


Figure 31 – SB 3 at failure

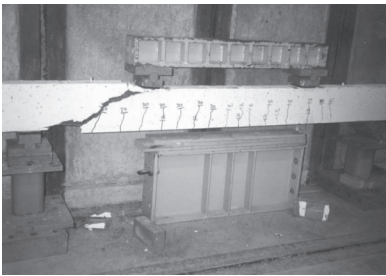


Figure 32 – SB 4 at failure

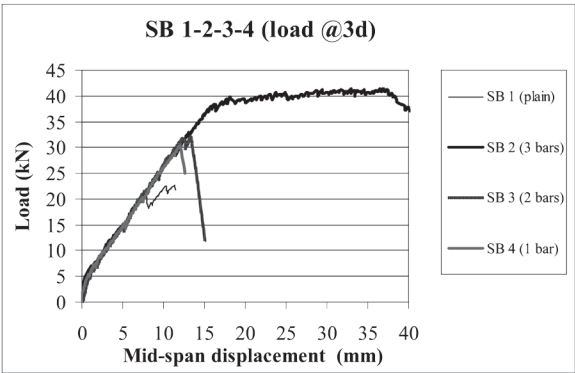


Figure 33 – Load-displacement plot for the FRP-strengthened beams

